TENTH AUSTRALASIAN FLUID MECHANICS
CONFERENCE - UNIVERSITY OF MELBOURNE
11-15 DECEMBER 1989

Keynote paper KS-5

NEW APPROACHES TO PROBLEMS IN FLUID MECHANICAL MIXING

A. LEONARD

Graduate Aeronautical Laboratories
California Institute of Technology
Pasadena, California 91125
USA

ABSTRACT

Problems of transport and mixing in fluid flows are considered, and it is shown how the methods of dynamical systems theory may be used in the analysis of these problems. Of particular interest are flows in which particle motions are chaotic in some region. Two general problems are considered - that of determining the fate of a blob of marked fluid (transport problem) and that of determining the fate of an interface in the flow (reacting flow problem).

For the case of time-periodic, two-dimensional flows mixing and transport is intimately related to the geometry of certain invariant curves in the Pomcaré map for the flow. The results are illustrated by considering the flow induced by a vortex pair in an oscillating strain-rate field. These invariant structures also dominate in flow visualization experiments because in some sense they act as an attractor. They are relatively easy to determine computationally from the velocity field.

1. INTRODUCTION

In most cases of interest, transport and mixing in fluid flows are dominated by convective processes so that the relative motions of fluid particles are all important. In particular, chaotic particle motions lead to greatly enhanced diffusion of mass, heat, and momentum and, in the case of reacting flows, greatly increased reaction rates. Such motions, while not possible in steady two-dimensional flows, are thought to be the rule rather than the exception because they are possible in time-dependent two-dimensional flows and even in steady three-dimensional flows.

In this paper it is shown that the methods and ideas of dynamical systems theory can be mobilized to provide powerful techniques for the analysis of particle transport and mixing in such flows. A sample of works along these lines includes Aref's (1984) investigation of a model flow system consisting of two "blinking" vortices and the study of chaotic streamlines in certain steady three-dimensional Euler flows by Dombre et al. (1986). More discussion and references are given in Ottino (1990). The present paper borrows heavily from the results of Rom-Kedar et al. (1989), hereafter called RLW, who have shown that transport in two-dimensional time-periodic flows is now reasonably well understood in terms of certain lobe-like structures appearing in the Poincaré map for the flow. This development is presented in Sec. 4 after introducing the example flow of an oscillating vortex pair in Sec. 2 and discussing the general features of the flow in Sec. 3. In Sec. 5 some results on interface dynamics in the example flow are presented and concluding remarks are presented in Sec. 6.

2. VORTEX PAIR IN A STRAINING FIELD

For illustrative purposes the two-dimensional flow governed by a vortex pair in the presence of an oscillating external strain-rate field (RLW) will be used. The vortices have circulations $\pm\Gamma$ and are separated by a nominal distance 2d in the y-direction. The stream function for the flow in a frame moving with the average velocity of the vortices is

$$\Psi = -\frac{\Gamma}{4\pi}\log\left[\frac{(x-x_v)^2+(y-y_v)^2}{(x-x_v)^2+(y+y_v)^2}\right] - V_v y + \bar{\varepsilon} xy \sin(\omega t) \tag{1}$$

where $(x_v(t), \pm y_v(t))$ are the vortex positions, $\bar{\varepsilon}$ is the strain-rate amplitude and V_v is the average velocity of the vortex pair. If $\bar{\varepsilon} = 0$ then $(x_v, y_v) = (0, d)$ and $V_v = \frac{\Gamma}{4\pi d}$. The equations of particle motion are

$$\frac{dx}{dt} = \frac{\partial\Psi}{\partial y} \qquad \frac{dy}{dt} = -\frac{\partial\Psi}{\partial x} \tag{2}$$

Each vortex moves under the influence of the other vortex and the straining field. Their equations of motion are easily integrated to give

$$x_v(t) = \exp\left[-\frac{\bar{\varepsilon}}{\omega}(\cos(\omega t)-1)\right] \int_0^t \left\{\frac{\Gamma}{4\pi d} - V_v \exp\left[-\frac{\bar{\varepsilon}}{\omega}(\cos\omega s)-1\right]\right\} ds \tag{3a}$$

$$y_v(t) = d\exp\left[-\frac{\bar{\varepsilon}}{\omega}(\cos(\omega t)-1)\right] \tag{3b}$$

where

$$V_v = \frac{\Gamma \exp(\bar{\varepsilon}/\omega)}{4\pi d\, I_o(\bar{\varepsilon}/\omega)} \tag{4}$$

There are two dimensionless parameters for this flow, the dimensionless strain-rate amplitude

$$\varepsilon = \tilde{\varepsilon}/\omega \qquad (5)$$

and the "Strouhal" period of the straining field

$$\gamma = \frac{\Gamma}{2\pi\omega d^2} \qquad (6)$$

3. PARTICLE MOTION - GENERAL OBSERVATIONS

For $\varepsilon = 0$, the flow is steady in a frame moving with the vortex pair. Typical streamlines are shown in Fig. 1 as well as the dividing streamline. Fluid particles and their trajectories are divided, by the dividing streamline, into two groups - those that are permanently trapped in a closed bubble moving with the pair and rotate on closed curves around a vortex and those that move in the fluid surrounding the bubble from upstream, around the bubble and then downstream. There is no exchange of fluid between the bubble fluid and the surrounding fluid. As shown in Fig. 2 a blob of marked fluid within the bubble must remain between the two bounding streamlines,

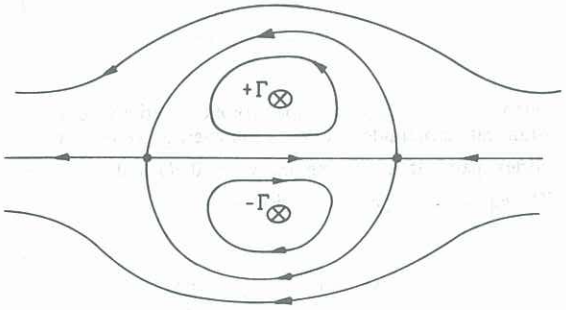

Figure 1 Streamlines for unperturbed flow.

forming a spiral structure with the number of turns in the spiral increasing linearly in time because of the different rotation rates of the particle trajectories between the two streamlines. Particle paths are not chaotic, i.e., the distance between two particles very close to one another initially does not increase at a sustained exponential rate but rather increases, in general, only linearly in time, as does a differential element of an interface.

For $\varepsilon \neq 0$, the situation changes considerably. The vortex trajectories are integrable (Sec. 2) and, in a fixed frame, are sketched in Fig. 3a. In a frame moving with the average speed of a vortex, the vortices move on closed elliptically-shaped curves but, as it will be shown, there are now three types of particle trajectories as illustrated in Fig. 3b. As before there are those particles that are permanently attached to a vortex and those that only pass by the vortex pair. However there is now an additional type of trajectory in which a particle approaches from upstream and then is "captured", encircling a vortex one or more times, before escaping downstream. In addition, the particle trajectories can be quite erratic (chaotic) in the vicinity of a vortex.

With regard to particle transport, reasonable questions of general interest might be:

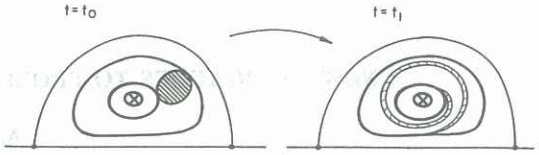

Figure 2 Evolution of a patch of marked fluid in the unperturbed flow.

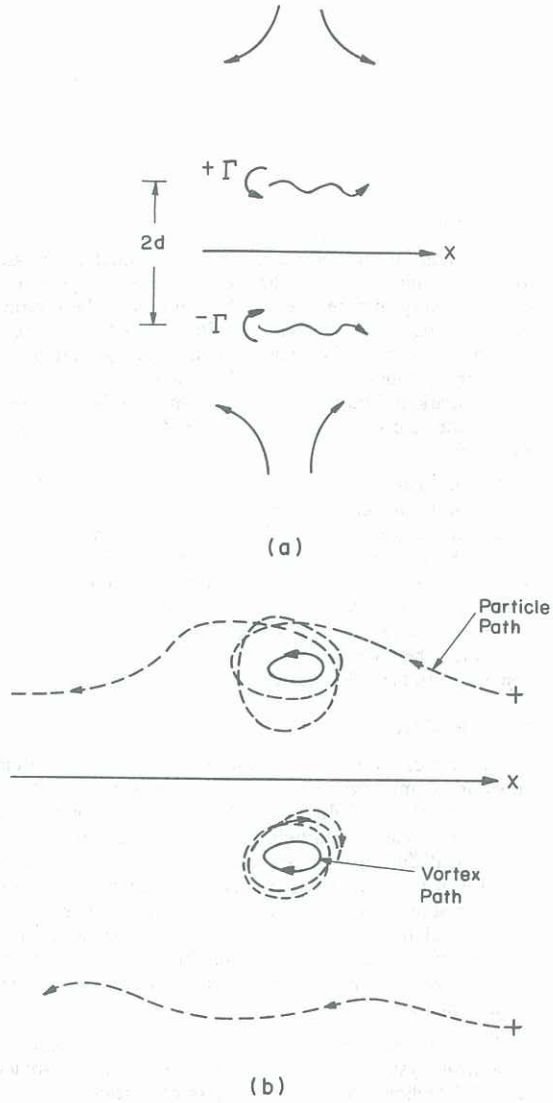

Figure 3 Motions in the perturbed flow. (a) Vortex motions in a fixed frame. (b) Vortex and particle motions in a moving frame.

1. What is the rate of capture or entrainment (area/time) as a function of ε and γ, and
2. For those particles that are captured, what is their distribution of residence times or times before escape?

These questions could be answered, of course, in a crude, brute force manner by integrating the equations of motion for a large group of particles, (i.e., approximating a three-dimensional continuum, two space plus time) and sampling the results. However, there is a much more efficient and elegant way to answer these questions as described in the next section.

4. POINCARE MAP - TRANSPORT MECHANISMS

A significant simplification of the description of particle motion is possible by using the Poincaré map - the map of the particle location $(x(t_o),\ y(t_o))$ to the location one period later $\rightarrow (x(t_o + 2\pi\gamma),\ y(t_o + 2\pi\gamma))$. For $\varepsilon = 0$, the map takes a point on a streamline and maps it onto another point on the same streamline as shown in Fig. 4a. There are two fixed points of the map, P_o and P_1, corresponding to the front and rear stagnation points, respectively, of the bubble. Both are hyperbolic fixed points so that passing through each is a collection of orbits forming a line that approaches P as $t \rightarrow +\infty$, called the

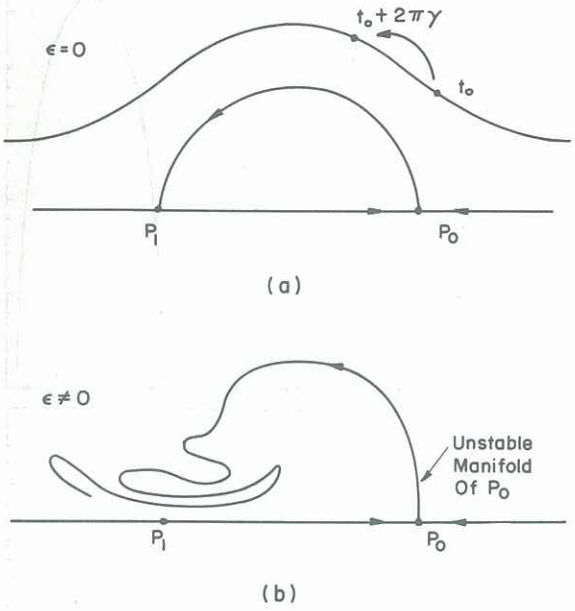

Figure 4 Invariant curves in the Poincaré map. (a) Unperturbed flow. (b) Perturbed flow.

stable manifold, and a collection of orbits that emanates from P (i.e., approaches P as $t \rightarrow -\infty$), called the unstable manifold. Note that in the unperturbed case the unstable manifold of P_o and the stable manifold of P_1 coincide and correspond to the limiting streamlines (Fig. 4a).

For $\varepsilon \neq 0$, the fixed points typically persist and the unstable manifold of P_o smoothly emanates from P_o as before but now undergoes strong oscillations as it approaches P_1 (Fig. 4b). To reveal the transport mechanism the stable manifold of P_1 must be determined as sketched in Fig. 5. (To compute the actual unstable and stable manifolds one locates P_o and P_1 respectively and then integrates forward (resp. backward) in time the motions of a collection of particles located initially close to P_o (resp. P_1) along the principal axis of expansion (resp. contraction).)

Note that the points A, B, C, D map to the points A', B', C', D'. In particular the cross hatched area surrounded by $ABCD$ is mapped to the other cross hatched area surrounded by $A'B'C'D'$. If the top half of a bubble of fluid is defined as that enclosed by P_oC on the unstable manifold of P_o, CP_1 on the stable manifold of P_1 and P_1P_o on the x-axis, then the cross hatched area ($ABCD$) is precisely that fluid that will be entrained into the bubble at the next cycle. Similarly the dotted area near A is that lobe that will be detrained from the bubble in the next cycle to the other dotted lobe near A'. Either one of the cross hatched lobes and its forward and backwards iterates define fluid in the *mixing zone*, i.e., fluid that has been or will be entrained (and ultimately detrained). Similarly either of the dotted lobes and its forward and

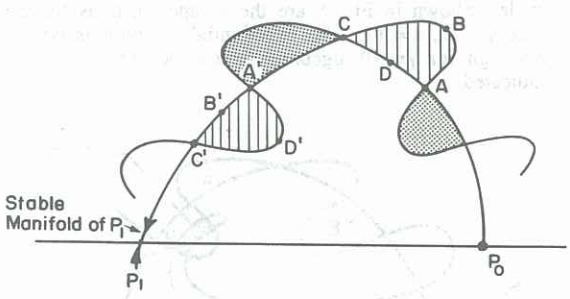

Figure 5 Portions of the unstable manifold of P_0 and the stable manifold of P_1 in the Poincare map for the perturbed flow.

backward iterates define the same mixing zone. Particle trajectories that fall within the mixing zone are those that encircle a vortex one or more times before escaping downstream.

For small ε the distance between the unstable and stable manifolds can be estimated by perturbation theory in terms of the Melnikov function (see Guckenheimer & Holmes (1983)). Thus one has an estimate of the width of the mixing zone near the vortices and, as shown by RLW, the entrainment rate, μ (E), to first order in ε, is given in terms of an integral of the Melnikov function. The entrainment rate vs. γ is sketched in Fig. 6. The rate achieves a maximum at $\gamma \approx 1.0$ but then drops to 0 (ε^2) for $\gamma \approx 1.4$ (for $\varepsilon = 0.1$) before rising again. This oscillatory behavior can be traced to the competing effects of vertical oscillations of the vortices, which are essentially independent of γ, and horizontal oscillations which increase with γ.

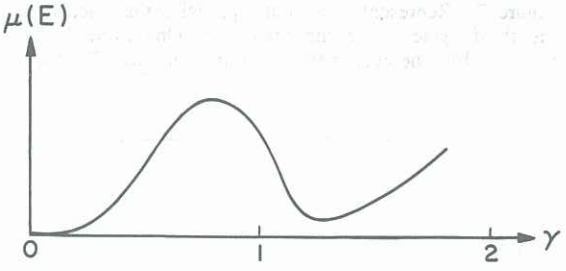

Figure 6 Entrainment area per cycle versus γ for $\varepsilon \neq 0$.

Within the bubble there is also fluid that is permanently trapped and therefore not in the mixing zone. For $\varepsilon \rightarrow 0$ or for $\gamma \rightarrow 0$ the area of this core fluid as a fraction of the bubble area approaches one. For $\varepsilon \neq 0$, the core fraction decreases for increasing γ then reaches a minimum. Curiously this minimum for $\varepsilon = 0.1$ is reached at $\gamma \approx 0.3$ (where the core fraction is ≈ 0.3) well below the γ where the entrainment rate is maximum (see RLW).

Fluid that is entrained into the bubble has a distribution of residence times for staying in the bubble. The lobe geometry also provides this information. As shown in the example illustrated in Fig. 7a, fluid during the first and second cycle of being entrained (lobes TE and T^2E as shown) is still completely contained within the bubble. However, the dotted area corresponding to the intersection of T^2E and the lobe D that will be detrained at the next cycle gives precisely the fluid that will escape at the third cycle. Fig. 7b shows where that fluid was located within the E lobe. Thus in general the intersection of $T^{k-1}E$ with D gives the area of fluid ($= e_k$) that requires k cycles to escape after entering the bubble on the first

cycle. Shown in Fig. 8 are the escape fractions for the case $\gamma = 0.5$, $\varepsilon = 0.1$. The exponential behavior is typical although for $\gamma = 0.9$ algebraic dependence of e_k on k is indicated.

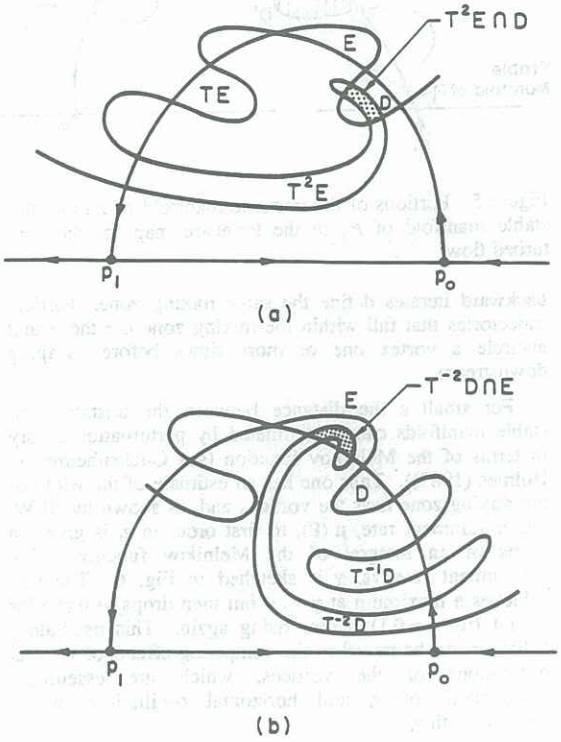

Figure 7 Representation of the particles that escape on the third cycle. T is the map. (a) One cycle before escape. (b) One cycle before entrainment (from RLW).

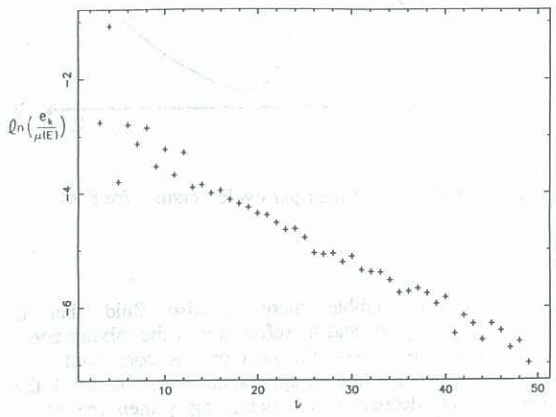

Figure 8 Escape fraction, $e_k / \mu(E)$, for the kth cycle versus k, $\gamma = 0.5$, $\varepsilon = 0.1$ (from RLW).

5. INTERFACE DYNAMICS

To convey the dramatic effect the unsteady flow has on an interface, the evolution, through six cycles, of an interface situated initially along the unperturbed dividing streamline is shown in Fig. 9 (Beige et al. (1989)). If $\varepsilon = 0$ the interface would of course remain as shown in Fig. 9a. For the case shown, $\gamma = 0.4$ and $\varepsilon = 0.1$, the evolution after three cycles, Fig. 9b, is not particularly striking. Note the three lobe structures of bubble fluid that have formed on the downstream side, separated by thin intrusions of outer fluid into the bubble region. However by six cycles the complexity of the interface has increased considerably. Again, the number of primary lobes forming the gross, outer boundary is six, corresponding to the number of cycles in the evolution, but the intrusions generally wrap around the vortex with excursions into the lobes and interrupted occasionally by a fold. This behavior is directly related to the fact that particle motion in the mixing zone within the bubble is chaotic as discussed below.

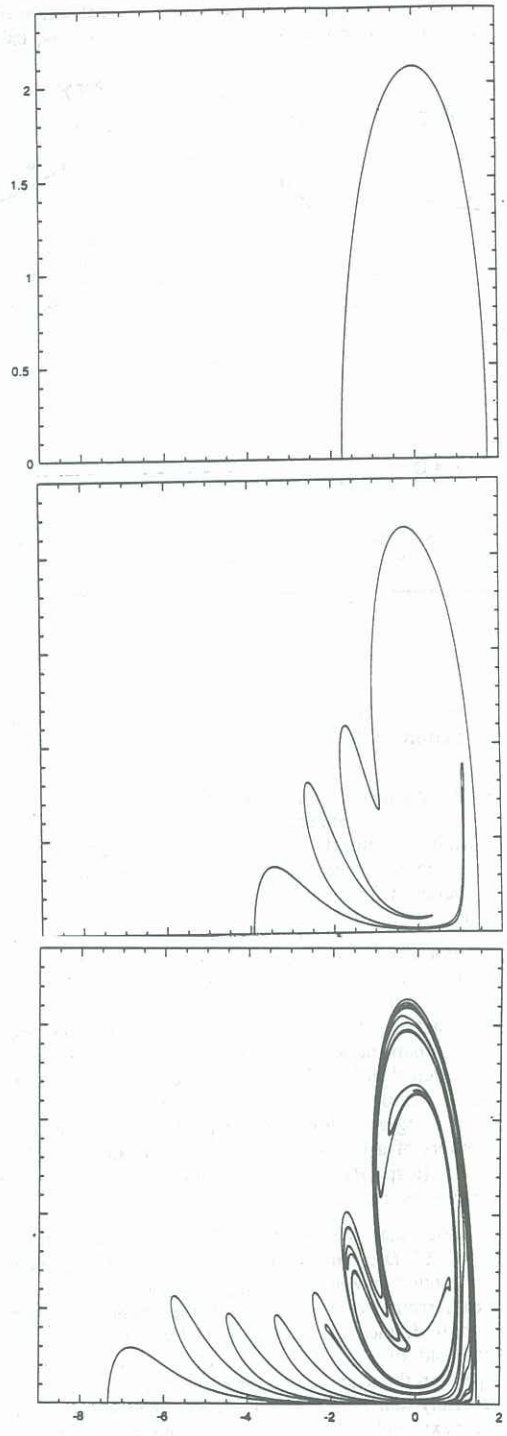

Figure 9 Evolution of an interface in the perturbed flow ($\gamma = 0.4$, $\varepsilon = 0.1$, located along the dividing streamline of the unperturbed case. (a) $t = 0$ (b) $t = 3(2\pi/\gamma)$ (c) $t = 6(2\pi / \gamma)$ (from Beigie et al. (1989)).

The quantitative information required concerning the interface depends on the problem at hand. Typically the local stretch history of the interface is of importance. As an example, if the interface is the flame sheet for a simple diffusion flame as discussed in Leonard et al. (1987) then the volume of reactant consumed per unit initial area of the sheet at point $\underline{p}$ is

$$V(\underline{p}, t) = \left[\frac{4D\tau}{\pi} \right]^{1/2} \tag{7}$$

Here D is the diffusion coefficient and τ is a time variable given by

$$\tau = \int_o^t S^2(\underline{p}, t')\, dt' \tag{8}$$

where S is the fractional increase in sheet surface area at $\underline{p}$. Thus knowledge of the distribution of S^2 as a function of time over the flame sheet should yield the total volume of reactant consumed. If the flow field is known or is being computed then such information is available also by brute force computation as illustrated below. On the other hand if a reasonable model for the stretching and folding of fluid elements can be constructed then such distributions may be computed directly from the parameters of the model (see, e.g., Ott and Antonsen (1989)). The missing link is the connection between the model parameters and the gross characteristics of the flow field of interest.

Unfortunately there are other complications to the diffusion flame problem and most any other reacting flow problem. The results given by (7) and (8) are valid only up to the point in time when the zone of the product at $\underline{p}$ collides with the product zone of another point on the sheet. Thus one must factor in global information about the sheet or, more specifically, *striation* thickness distributions. One must also consider the motion of the flame sheet relative to the material interface. An effort along these lines has been made by Muzzio and Ottino (1989) who consider the evolution of striation thickness distributions in one-dimensional systems without stretching.

Consider the problem of determining the stretch of an element of a material interface. If $\underline{\delta}(t)$ is differential vector element of a material interface in a two-dimensional potential flow, then $\underline{\delta}$ evolves according to

$$\frac{d\underline{\delta}}{dt} = \begin{bmatrix} a(t) & b(t) \\ b(t) & -a(t) \end{bmatrix} \underline{\delta} \tag{9}$$

where

$$a = \frac{\partial u}{\partial x} = -\frac{\partial v}{\partial y} \tag{10a}$$

$$b = \frac{\partial u}{\partial y} = \frac{\partial v}{\partial x} \tag{10b}$$

and are evaluated at the location of the interface element. The total stretch or elongation of an element at time t is clearly

$$S = |\underline{\delta}(t)| \,/\, |\underline{\delta}(0)| \tag{11}$$

In Fig. 10 the log of the total stretch versus time for a particular line element that escapes the bubble region after 12 cycles is shown. The erratic stretching during the time the element is within the bubble is followed by an interval of smooth stretching as the element escapes and moves past the rear stagnation region. The element ultimately elongates by a factor of $\simeq \exp[14] \simeq 1.2 \times 10^6$. If the element is part of a flame sheet then the information given in Fig. 10 is sufficient to compute the volume of reactant consumed/area at that point by equations (7) and (8). With the crude approximation $S \simeq \exp(t/2\pi\gamma)$ for $t/2\pi\gamma \leq 14$ it is found that the ratio of reactant volume consumed with stretching to that consumed without stretching is

$$[\tau/t]^{1/2} \simeq \frac{\exp(t/2\pi\gamma)}{(t/\pi\gamma)^{1/2}} \tag{12}$$

When $t/2\pi\gamma = 14$ this ratio is approximately 2×10^5.

The example given in Fig. 10 is not unusual. By following a number of elements until they escape and complete their elongation one obtains a broad distribution

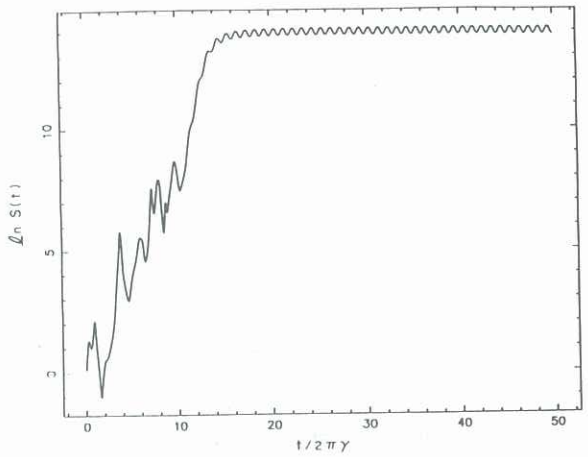

Figure 10 Stretch or elongation versus time experienced by a particular line element that escapes after 12 cycles $\gamma = 0.5$, $\varepsilon = 0.1$ (from RLW).

of elongations as shown in Fig. 11. By averaging the logarithms of the elongations for elements having the same escape cycle, a clear indication of exponential increase in stretch with residence time is obtained as shown in Fig. 12. The vertical offset or constant factor is presumably due to the elongation suffered after escape.

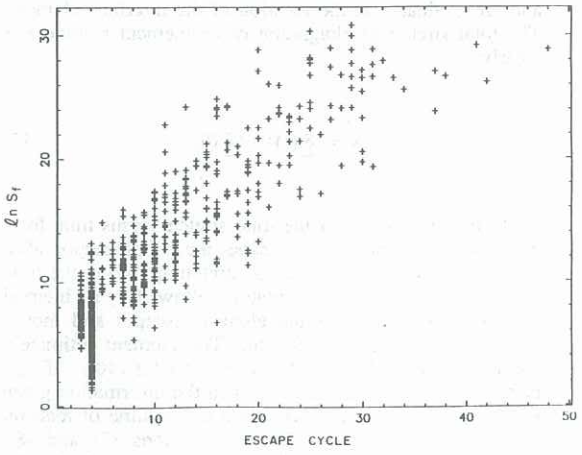

Figure 11 Final elongation after escape for 530 line elements versus time of escape (from RLW).

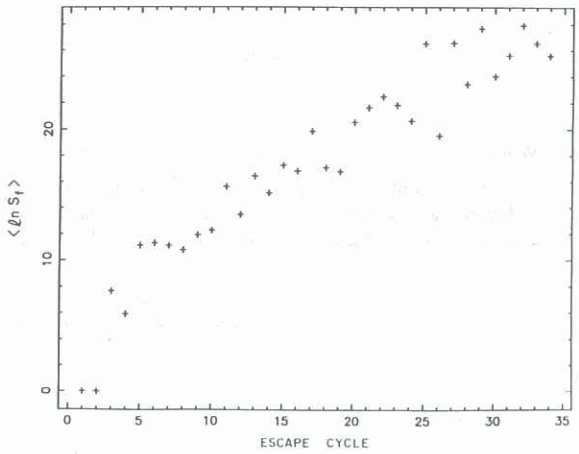

Figure 12 Average log elongation of data shown in Figure 11 (from RLW).

6. SUMMARY AND CONCLUSIONS

The complexity of the transport of particles undergoing chaotic motions in a two-dimensional, time-periodic flow has been reduced considerably by considering certain invariant curves in the Poincaré map for particle motion. Lobe-like structures govern entrainment into and detrainment from particular regions in the flow and determine residence time distributions for particles entrained into these regions.

As expected, the geometry of an interface becomes increasingly complex as it remains within a chaotic zone because of the continual stretching and folding of material lines. By direct computation, a broad distribution in the average stretch rate was found for a group of line elements in the flow considered. Such distributions are likely to be typical. It would be very desirable to be able to predict the distribution of stretch rates given only general characteristics of the flow.

Other future research efforts might focus on extending the above results to (1) more general time dependence (see Beigie et al. (1989)), (2) three dimensions, and (3) the general problem of defining and computing the successor to the turbulent eddy diffusivity.

REFERENCES

AREF, H. (1984) Stirring by Chaotic Advection, *J. Fluid Mech.*, **143**, pp. 1-21.

BEIGIE, D., LEONARD, A. and WIGGINS, S. (1989) Chaotic Transport in the Homoclinic and Heteroclinic Tangle Regions of Quasiperiodically Forced Two Dimensional Dynamical Systems, Caltech preprint.

DOMBRE, T., FRISCH, U., GREENE, J. M., HENON, M., MEHR, A. and SOWARD, A. (1986) Chaotic Streamlines in the ABC Flows, *J. Fluid Mech.*, **167**, pp. 353-391.

GUCKENHEIMER, J. and HOLMES, P. (1983) *Non-Linear Oscillations, Dynamical Systems and Bifurcations of Vector Fields*, Springer-Verlag, New York.

LEONARD, A., ROM-KEDAR, V. and WIGGINS, S. (1987) Fluid Mixing and Dynamical Systems, *Nucl. Phys. B. (Proc. Suppl.)*, **2**, pp. 179-190.

MUZZIO, F. J. and OTTINO, J. M. (1989) Evolution of a Lamellar System with Diffusion and Reaction: A Scaling Approach, *Phys. Rev. Lett.*, **63**, pp. 47-50.

OTT, E. and ANTONSEN, JR., T. M. (1989) Fractal Measures of Passively Convected Vector Fields and Scalar Gradients in Chaotic Fluid Flows, *Phys. Rev. A*, **39**, pp. 3660-3671.

OTTINO, J. M. (1990) Mixing, Chaotic Advection, and Turbulence, *Ann. Rev. Fluid Mech.*, **22**, pp. 207-254.

ROM-KEDAR, V., LEONARD, A. and WIGGINS, S. (1989) An Analytical Study of Transport, Mixing and Chaos in an Unsteady Vortical Flow, *J. Fluid Mech.*, (to appear).